Analysis of the Dynamic Response Mechanism of Rock Slopes Based on Numerical Simulation

Yunhan Hou[1, #], Wenjie Zhao[2, #], Chenguang Wang[2, #, *]

[1]School of Architecture and Construction, Sichuan Agricultural University, Chengdu, China, 611830

[2]School of Management Engineering, Qingdao University of Technology, Qingdao, China, 266520

*Corresponding author: WCG3169518927@163.com

#These authors contributed equally.

Abstract. Rock slopes are widely distributed in China's strong seismic areas, and due to the wide distribution of seismic areas in China and frequent seismic activities, there is an urgent need to carry out scientific research on the dynamic response of slopes. This paper aims to use the discrete element method to simulate three different earthquake waves on a simplified model and analyse and evaluate the results based on the visual images obtained from the experiment. The results show that the maximum displacement is concentrated at the bottom of the slope model, indicating that the bottom of the slope is most vulnerable to damage under earthquake action. In practical engineering, the state of the construction slope should be monitored in real time to reduce losses caused by earthquakes and other damage. In this study, the effects of different seismic waves on the dynamic response of slopes were investigated to lay the foundation for subsequent studies on the stability of slopes in multi-subsequent earthquakes.

Keywords: Rock Slope; Seismic Wave; Dynamic Response; Numerical Simulation.

1. Introduction

In today's world, where natural disasters are frequent, earthquakes are one of the most destructive natural disasters. Not only do they directly threaten human lives, they also cause huge economic losses and social impacts by damaging infrastructure. China is located at the intersection of the Pacific Rim seismic belt and the Eurasian seismic belt. It is subject to multiple compressions from the Pacific, Indian and Philippine Sea plates, and the earthquake fault zones are active. As major national projects advance into complex geological environments, the issue of slope stability is particularly prominent in mountainous and hilly areas— especially in major earthquakes such as the Wenchuan Earthquake and the Nepal Earthquake. The horizontal and vertical two-way shaking caused by seismic waves causes the geotechnical body to loosen and slide, inducing secondary disasters such as landslides and collapses, whose destructive power can even exceed that of the earthquake itself. The traditional static stability assessment of slopes is no longer sufficient to deal with the complexity of seismic dynamic loads. This dynamic effect can change the stress state and structural characteristics of the geotechnical body, exacerbating the risk of slope instability. Therefore, an in-depth study of the dynamic response mechanism of slopes under seismic action is not only an urgent need to protect people's lives and property, but also an important topic to support the construction of major national projects and promote the development of geotechnical engineering.

2. Background information

Current research on the seismic response of rock slopes mainly relies on three major methodological systems: theoretical analysis, experimental simulation and numerical simulation. Among these, numerical simulation technology has become the focus of research due to its high efficiency and adaptability to complex factors. For example, the Finite Element Method [1] (FEM): solves stress, strain and displacement parameters by dividing into small units, and is suitable for dynamic response analysis of complex media and topographic conditions. Its advantage is that it can handle complex geometries and is often used to study the overall behaviour of slopes under seismic

action. Discrete Element Method [2] (DEM): Based on the contact between rigid blocks/particles, the displacement, velocity and other parameters are obtained by solving the equation of motion of the blocks. It has significant advantages in geological and mining engineering. Boundary Element Method [3] (BEM): based on the boundary integral equation, the global problem is solved by discretising the boundary. It has outstanding advantages when dealing with infinite/semi-infinite domain slope problems. Fast Lagrangian Analysis of Continua [4] (FLAC): uses explicit finite difference technology and is good at simulating large deformations and material nonlinear behaviour. Monte Carlo simulation method [5]: generates probability distributions by statistically random variables to assess the risk of slope instability. It is suitable for stability analysis that considers the uncertainty of geotechnical parameters and can comprehensively consider the influence of multiple factors. Discontinuous Deformation Analysis [6] (DDA): This method is used to simulate rock mass displacement and failure with discontinuous surfaces such as joints and faults. In addition, the GRA-TOPSIS evaluation model [7] improves the accuracy of stability assessment of complex systems through variable weight theory and grey relational analysis, while the theory of sharp point mutation [8] analyzes the critical state of slope instability from the mathematical model of catastrophe. Field monitoring forms a feedback loop through time series analysis, risk modeling and data visualization [9], providing a basis for verification of numerical simulation. The multi-dimensional collaboration of numerical methods is driving the research on slope seismic resistance from a single mechanical analysis to an intelligent development of the whole chain of 'mechanism-prediction-prevention and control'.

Although scholars at home and abroad have made significant progress in the field of seismic slope stability, they still face three core challenges: the nonlinear coupling mechanism between ground shaking parameters and the dynamic response of slopes has not yet been fully revealed, which leads to limited prediction accuracy; the quantitative model of slope instability threshold under the action of multi-field coupling [10] (seismic-percolation-geological tectonics) lacks universality; and the engineering adaptability and long-term reliability of anti-vibration reinforcement technology under complex geological conditions need to be improved. The engineering adaptability and long-term reliability of anti-vibration reinforcement technology under complex geological conditions need to be improved. To this end, this study integrates the latest theories and typical earthquake cases, and builds a research system of "Mechanism Analysis-Efficacy Verification-Technology Optimization": based on the analysis of energy transfer paths and progressive damage characteristics, a three-dimensional dynamic stability evaluation model for geologically heterogeneous slopes is established; combined with BIM numerical simulation and intelligent monitoring feedback, the research and development of the integrated pre-stressing anchor cable group cooperative dissipation model is developed. Combined with BIM numerical simulation and intelligent monitoring feedback, the design method of toughness reinforcement incorporating the cooperative energy dissipation technology of prestressing anchor cable group is developed. The research results will form a complete chain from theoretical modeling to engineering application, providing solutions with both prediction accuracy and resilience for slope projects in high-risk areas of earthquakes.

3. Research flowchart

In this experimental study, a generalised slope model of a half-infinite space will be established, and the model will then be imported into the FLAC3D software. By studying the effects of different seismic waves on the model profile and collecting experimental data with the software, the experimental data will be analysed and processed to understand the relevant changes of the slope model under the action of seismic waves. The specific research process is shown in the Figure 1.

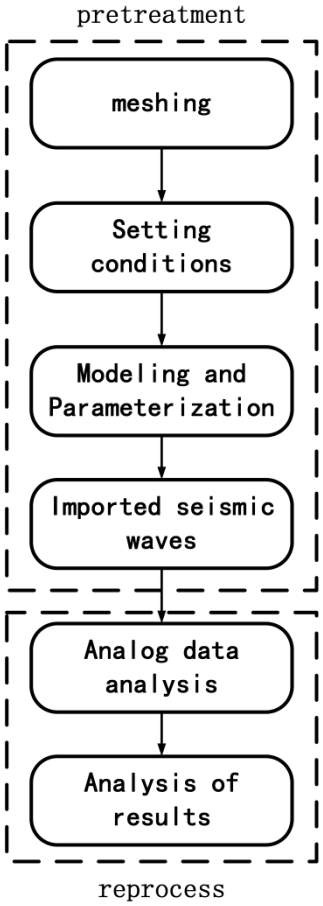

Figure 1. Research flowchart

3.1. Grid division

Before a model can be built for analysis, it must first be meshed. The accuracy and reliability of the seismic analysis of slopes can only be guaranteed if the mesh size is less than 1/8-1/10 the wavelength corresponding to the highest input seismic frequency. This is expressed by the formula:

$$\Delta l \le \left(\frac{1}{10} \sim \frac{1}{8}\right)\lambda \tag{1}$$

Δl——Grid size;

λ——Enter the wavelength corresponding to the maximum seismic frequency, which can be calculated using the following formula:

$$\lambda = \frac{C_s}{f} \tag{2}$$

f——Enter the maximum seismic frequency;

Cs——Enter the seismic shear wave velocity, which is calculated using the following formula:

$$C_s = \sqrt{\frac{E}{2\rho(1+v)}} = \sqrt{\frac{G}{\rho}} \tag{3}$$

E——Slope modulus of elasticity;

ρ——Slope density;

υ——Slope Poisson's ratio;

G——Slope shear modulus;

After processing and calculating the data, the value of the grid size of the model selected in this case is 1m.

3.2. Boundary condition setting

This seismic dynamic simulation of the slope will be carried out with the help of a built-in program in FLAC3D. The relevant parameter settings for the program are as follows:
In the FLAC3D program, there are three built-in damping methods: local damping, Rayleigh damping and hysteretic damping.

Since the research model established this time is a generalised model that is relatively simple, and local damping is not sensitive to frequency, it can achieve good simulation results in simple models. Therefore, local damping should be considered during dynamic loading.

The characteristics of local damping are suitable for dynamic simulation. The working principle is that while the overall mass is conserved, the mass on a grid node on the model changes during an oscillation cycle. Usually, an increase in mass is indicated by a change in speed, while a decrease in mass is indicated by the speed reaching a maximum or minimum. Therefore, the kinetic energy increment decays twice during each oscillation cycle. The energy lost in this process is proportional to the maximum instantaneous strain energy, and the ratio of the two can be expressed in terms of the critical damping fraction as follows:

$$\alpha_L = \pi D \tag{4}$$

α_L——Local damping factor;
D——Critical damping ratio;
The critical damping ratio in this paper is taken as 0.05
The local damping coefficient in this simulation is 0.157

In order to reduce the reflection of energy on the boundary in the simulation experiment, the FLAC3D built-in free-field boundary is set around the model, which can have the effect of reducing the reflected waves at the model boundary.

The free-field boundary is a setup where the lateral boundary of the body mesh and the free-field mesh are coupled by a damper to apply the unbalanced force of the free-field mesh to the boundary of the body mesh.

The applied force can be calculated by the following equation:

$$F_{\mathrm{x}} = -\rho C_{\mathrm{p}} \left(v_{\mathrm{x}}^{\mathrm{m}} - v_{\mathrm{x}}^{\mathrm{ff}} \right) A + F_{\mathrm{x}}^{\mathrm{ff}} \tag{5}$$

$$F_{y} = -\rho C_{\mathrm{p}} \left(v_{\mathrm{y}}^{\mathrm{m}} - v_{\mathrm{y}}^{\mathrm{ff}} \right) A + F_{\mathrm{y}}^{\mathrm{ff}} \tag{6}$$

$$F_{\mathrm{z}} = -\rho C_{\mathrm{p}} \left(v_{\mathrm{z}}^{\mathrm{m}} - v_{\mathrm{z}}^{\mathrm{ff}} \right) A + F_{\mathrm{z}}^{\mathrm{ff}} \tag{7}$$

In the above equations, $F_{\mathrm{x}}^{\mathrm{ff}}$, $F_{\mathrm{y}}^{\mathrm{ff}}$ and $F_{\mathrm{z}}^{\mathrm{ff}}$ denote the nodal forces of the free-field grid; $v_{\mathrm{x}}^{\mathrm{m}}$, $v_{\mathrm{y}}^{\mathrm{m}}$, and $v_{\mathrm{z}}^{\mathrm{m}}$ denote the velocities of the main grid in the corresponding directions on the lateral boundaries; $v_{\mathrm{x}}^{\mathrm{ff}}$, $v_{\mathrm{y}}^{\mathrm{ff}}$, and $v_{\mathrm{z}}^{\mathrm{ff}}$ denote the velocities of the lateral free-field grids in the corresponding directions on the connecting boundaries; ρ denotes the density of the material at the boundary of the mould in the vertical direction; A denotes the area of influence of the free grid; Cp and Cs denote the propagation velocities of compression and shear waves at the lateral boundaries in the modelled medium, respectively.

In order to make the simulation experiment close to the real effect and simulate the real situation of the earthquake, this simulation will choose the way of acceleration time course input.And the dynamic load is only applied in the X-direction of the model, and its applied values are 0.1g,0.5g,1.0g in order.

3.3. Modelling and related parameters

The specific arrangement of this generalized slope model is shown in Figure 2, and the relevant physical parameters of the model are shown in Table 1. (refer to the Rock and Soil Mechanics Parameters)

Table 1. Generalize the physical parameters of the slope

Nature of material	Density /(g/cm^3)	Bulk modulus /(GPa)	shear modulus /(GPa)	angle of internal friction/(˚)	cohesion/(MPa)	tensile strength /(MPa)
Soil	2.67	3.99	2.01	23	2	1.5

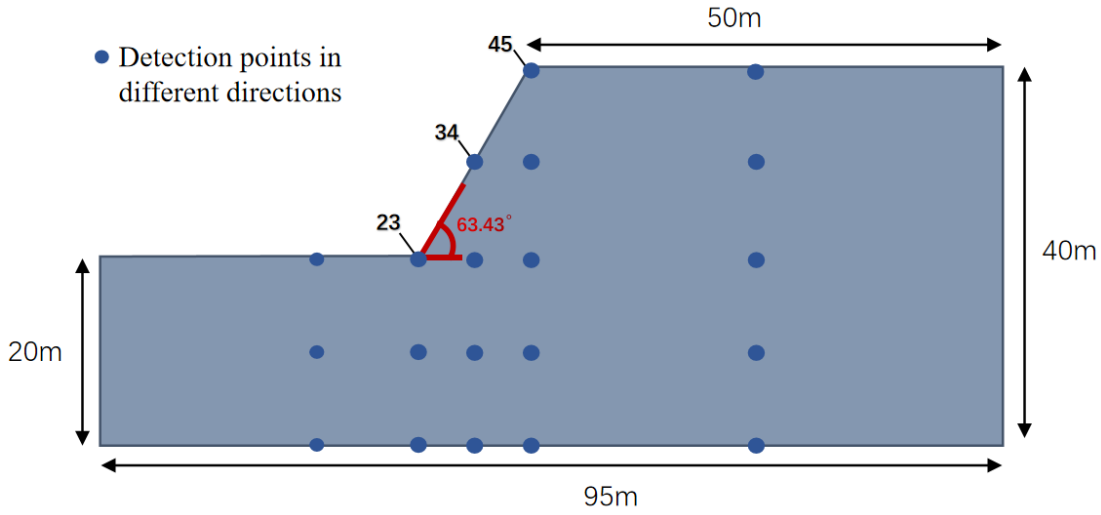

Figure 2. Sketch of the generalized model and detection points

3.4. Importing seismic waves

In this numerical simulation, selected seismic waves detected in Luding, Wolong and Lushan are used as input seismic waves, which act on the bottom of the model in the horizontal and vertical directions, with peak accelerations of 0.1g, 0.5g and 1.0g, and the duration of their action times of 7S, 7.5S, and 10S, respectively, and their correlation frequencies are shown in Figures 3.

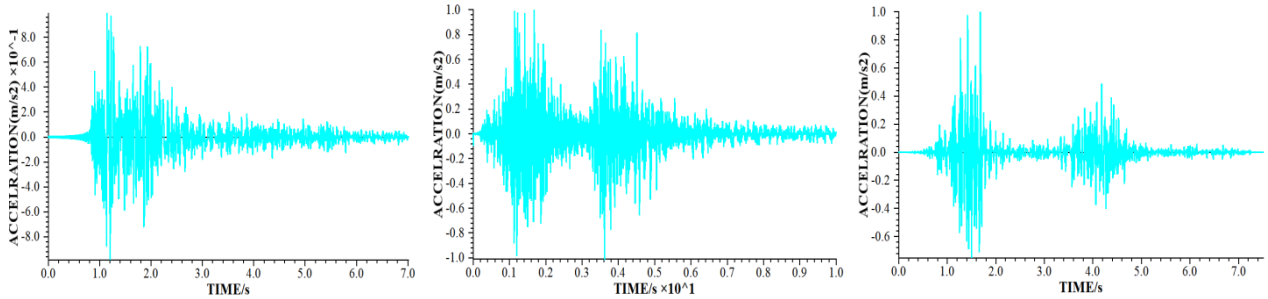

Figure 3. Three types of seismic waveforms

4. Data analysis

Simulation experiments on the generalized model using three different seismic waves to obtain the values of acceleration, displacement and stress analysis, and to draw visual pictures of the data to analyze and evaluate the experimental results.

4.1. Stress analysis of slope shoulder under different input accelerations

Taking the shoulder of the model slope as the observation object, the maximum shear stresses at this point under different input accelerations are organized and collected. The relevant information is shown in Figure 4. At an initial acceleration of 0.1g, the three seismic waves produced analogous values of maximum shear stress on the slope shoulder (approximately 7.5 kPa). As the input

acceleration increases to 1g, the stress values exhibit a substantial increase, and the variability increases concomitantly. The Luding wave generates the smallest maximum stress value (approximately 17 kPa), whilst the Lushan and Wolong waves demonstrate a comparable trend, producing a maximum stress value of 19 kPa.

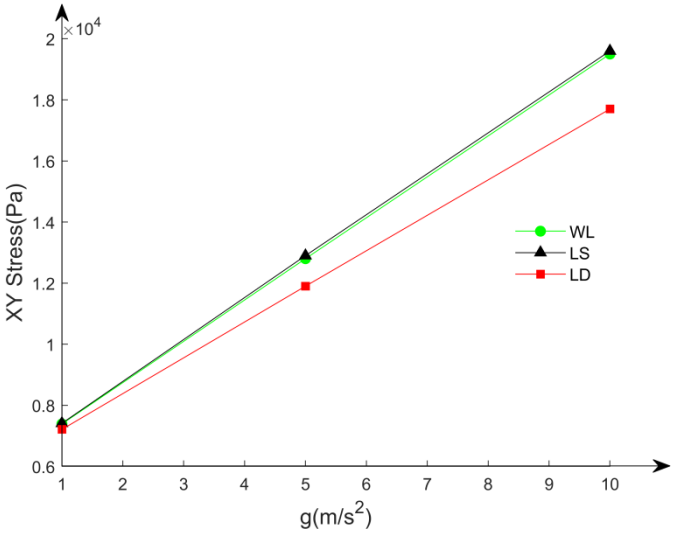

Figure 4. Slope shoulder stress changes under different input accelerations of three seismic waves

4.2. Analysis of slope shoulder acceleration with different input accelerations

The numerical analysis of acceleration in the x-axis and z-axis directions is carried out for the slope shoulder point. The relevant information is shown in Figure 5 and Figure 6. At 0.1g, the three seismic waves produce very similar values of maximum acceleration on the x-axis, which is about 2.5m/s^2. The same situation exists on the z-axis. As the input acceleration increases, the maximum acceleration values in the x-axis and z-axis increase accordingly. At 1g, the maximum acceleration values of the three seismic waves in the x-axis direction are about 26m/s^2, 25m/s^2 and 24m/s^2, respectively. in the z-axis direction, the values of the Wolong and Lushan seismic waves are similar, while the value of the Luding seismic wave is about 16m/s^2.

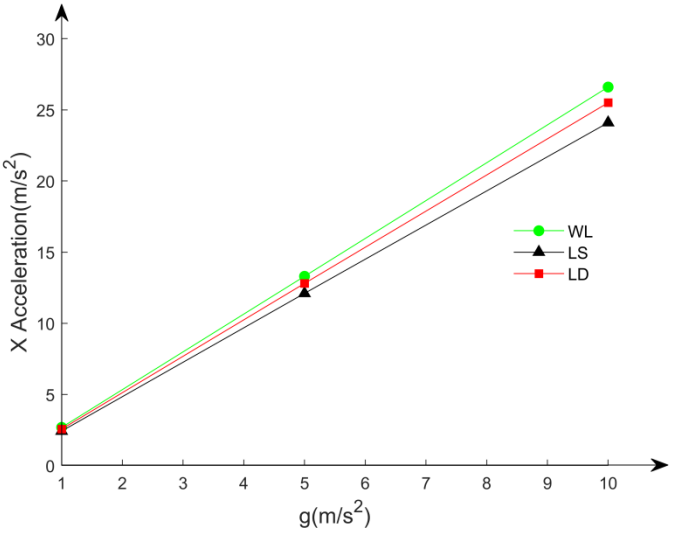

Figure 5. X-direction acceleration of slope shoulder with different input accelerations of three seismic waves

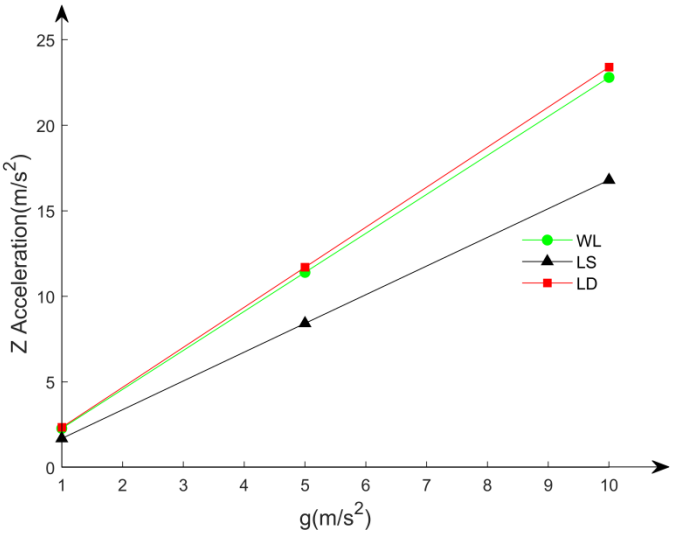

Figure 6. Z-direction acceleration of slope shoulder with different input accelerations of three seismic waves

4.3. Slope shoulder displacement analysis with different input accelerations

The displacement analysis of the slope shoulder point was subsequently conducted in the x-axis and z-axis directions. The relevant information is shown in Figures 7 and 8. At 0.1g, the displacement value caused by the Luding seismic wave on the x-axis is close to 0 and the subsequent change is very slow, while the remaining two seismic displacements change in a very similar way, with their values rising as the input acceleration rises, and the final value is in the vicinity of 0.034 m. The displacement values of the Luding seismic wave on the z-axis follow a similar rate of change. On the z-axis, the displacement values of the three seismic waves follow a similar rate of change and rise steadily, with the Wolong and Lushan seismic waves producing similar maximum acceleration values of about 0.91 * 10^{-3} m. The Luding seismic wave is about 0.75 * 10^{-3} m.

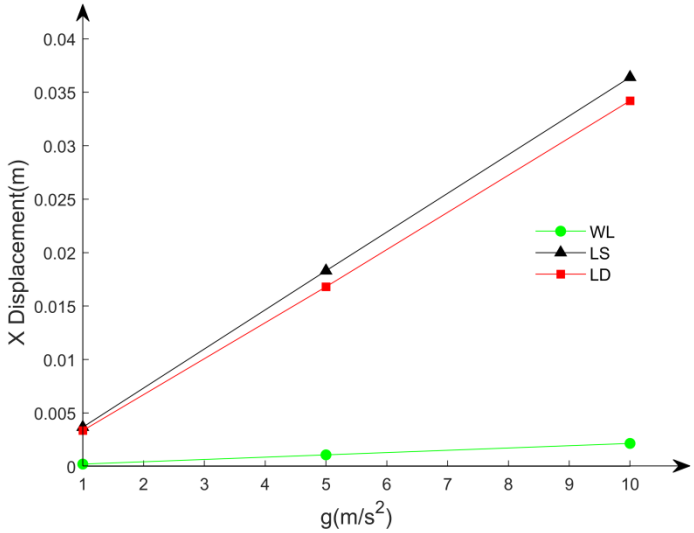

Figure 7. X-direction displacement of slope shoulder for three seismic waves with different input accelerations

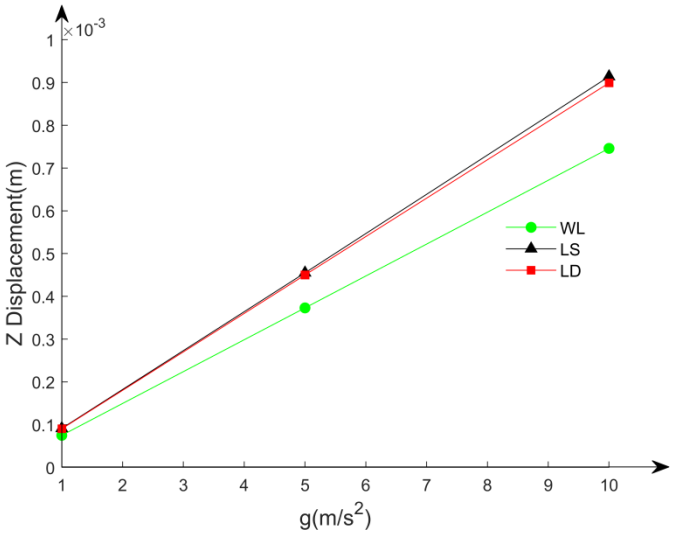

Figure 8. Z-direction displacement of slope shoulder for three seismic waves with different input accelerations

4.4. Comparison of acceleration at the shoulder and bottom of the slope for different seismic waves

Subsequently, the study analyzes the numerical changes in acceleration under the influence of three seismic waves at two observation points, the shoulder and the bottom of the slope. The relevant information is shown in Figure 9.

Initially, the Luding seismic wave is analysed. From the general outline of the waveform, it is evident that the larger acceleration values are concentrated in the first 4 seconds of the seismic wave. Furthermore, it is observed that, irrespective of the direction of acceleration in the X-axis or Z-axis, the acceleration at the shoulder of the slope is significantly higher than that at the bottom of the slope in terms of both the peak value and the average value. The peak acceleration values at the shoulder in the x-axis direction are 2.56m/s^2, 12.77m/s^2, 25.50m/s^2, and the peak acceleration values at the bottom of the slope are about 2.26m/s^2, 11.30m/s^2, 22.64m/s^2. In the z-axis direction, the peak acceleration values at the shoulder of the slope are 2.34m/s^2, 11.70m/s^2, 23.41m/s^2, and the peak acceleration at the bottom of the slope are 0.98m/s^2, 4.91m/s^2, 9.75m/s^2.

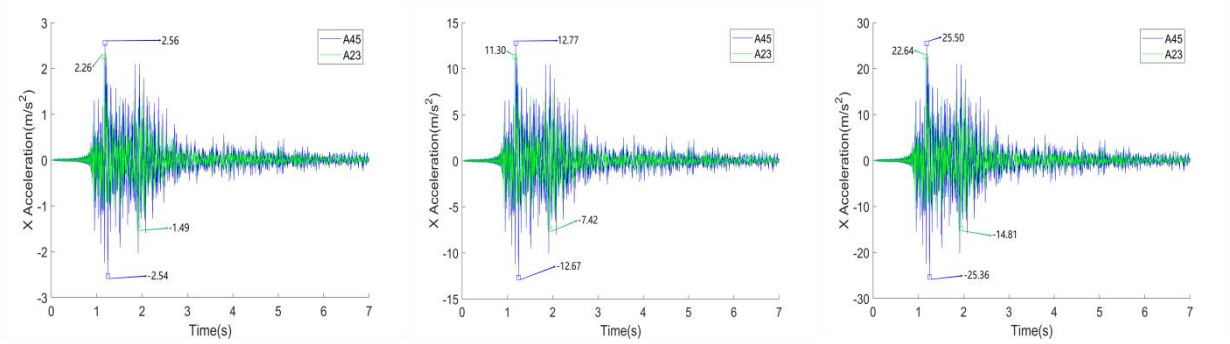

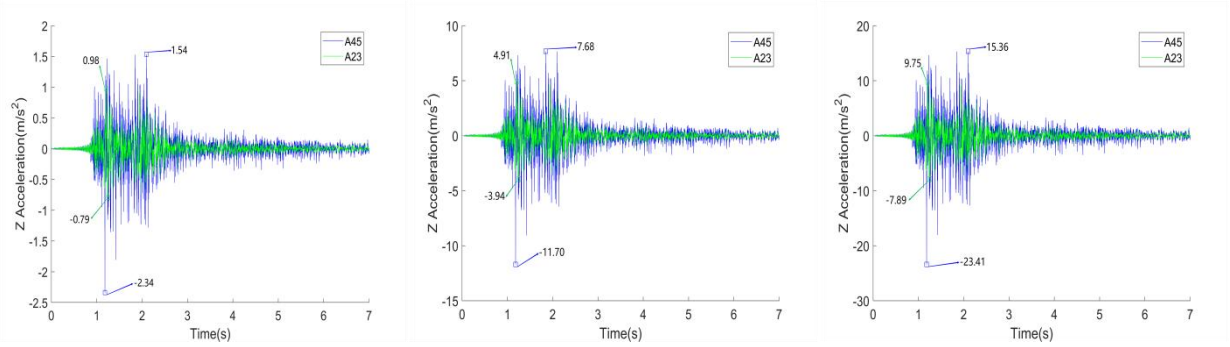

Figure 9. Comparison of slope shoulder and bottom acceleration under the influence of LD seismic waves

The Lushan seismic wave was subsequently analysed. The relevant information is shown in Figure 10. The larger acceleration values manifest in the middle segment of the seismic wave between 4 and 8 seconds, and the peak acceleration at the shoulder of the slope exceeds that at the base of the slope in both the x- and z-axis directions. A comparison of the waveforms reveals a similarity between the Lushan and Luding seismic waves in the segment of the highest acceleration interval. Consequently, the numerical changes of the slope shoulder and the slope bottom detected by the Lushan wave are highly analogous to those of the Luding wave above.

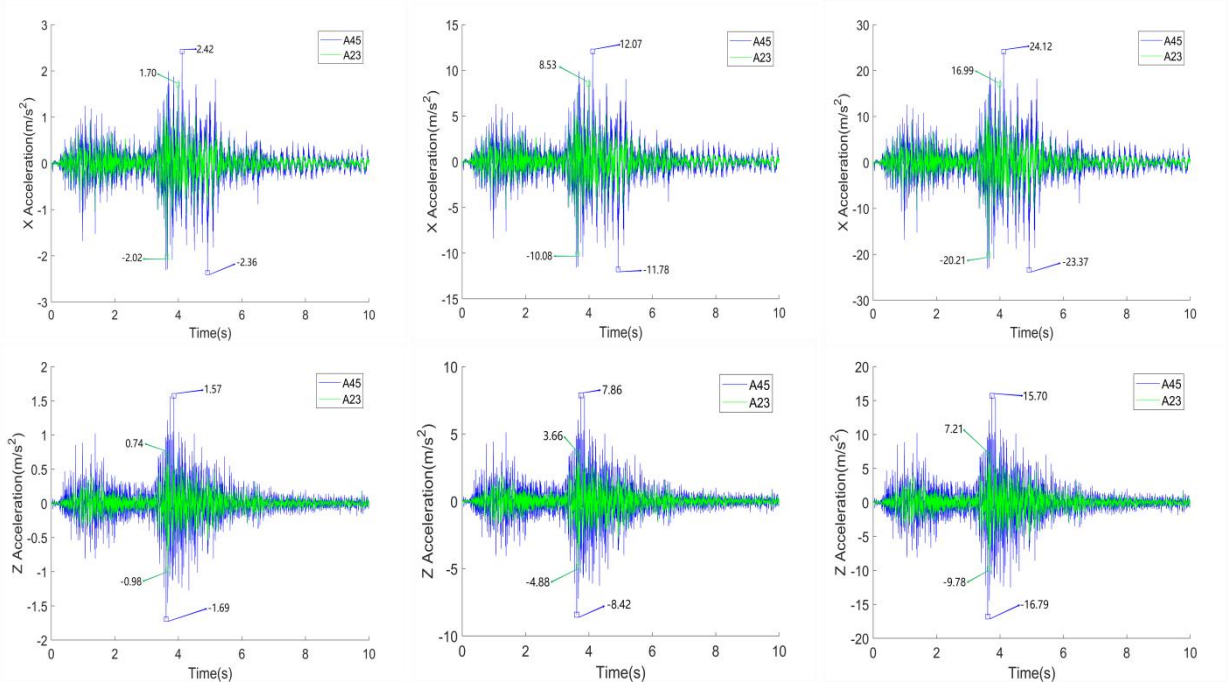

Figure 10 Comparison of slope shoulder and base acceleration under the influence of LS seismic waves

In conclusion, an analysis of the seismic waves in Wolong is presented. The relevant information is shown in Figure 11. The larger acceleration values are concentrated in two time periods: 2 to 4 seconds and 5 to 7 seconds. Furthermore, the acceleration values in the x- and z-axis directions reveal that the peak acceleration at the shoulder of the slope exceeds that at the base. Specifically, the peak acceleration in the x-axis direction at the shoulder of the slope is approximately 1.7 times the peak acceleration at the slope's base. Furthermore, a more pronounced disparity in data is observed when comparing the z-axis direction, with the peak acceleration at the shoulder of the slope reaching almost twice that of the peak acceleration at the slope's base.

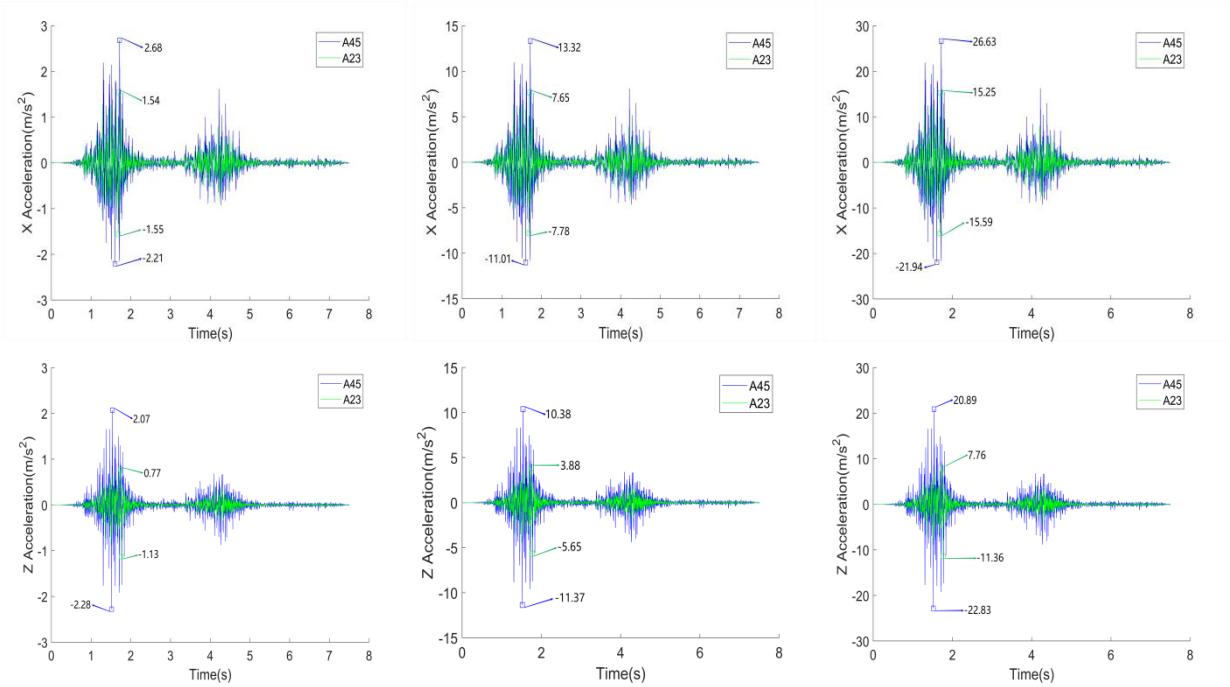

Figure 11. Comparison of acceleration at the shoulder and bottom of a slope under the influence of WL seismic waves

4.5. Displacement and stress analysis of the model as a whole under different seismic waves

The experimental data derived from this model were then utilised to generate cloud maps, which were employed for the analysis of displacement changes and stress values of the model in response to the action of seismic waves.

The experimental analysis of the Luding seismic wave is the first element of the study. The information is shown in Figure 12. As the input acceleration value increases, the maximum displacement of the model also increases, and this increase is very significant. The maximum displacement in this data set is about 8.7 times the minimum displacement. A thorough examination of the cloud diagram reveals that the maximum displacement value is predominantly concentrated in the slope shoulder of the slope model. This observation suggests that the shoulder region is particularly vulnerable to damage during seismic events.

Observe the stress cloud diagram of the slope model. The relevant information is shown in Figure 12. The maximum stress value of the model is $1.32*10^5$Pa, $1.33*10^5$Pa, $1.34*10^5$Pa when the model inputs acceleration 0.1g, 0.5g, 1.0g. The model at the bottom of the slope will be more damaged than the upper sections. The maximum stress of the model is carried at the bottom of the model slope. Therefore, in practice, we need to pay attention to the stress situation at the bottom of the slope to avoid exceeding the pressure threshold of the rock and soil at the bottom of the slope.

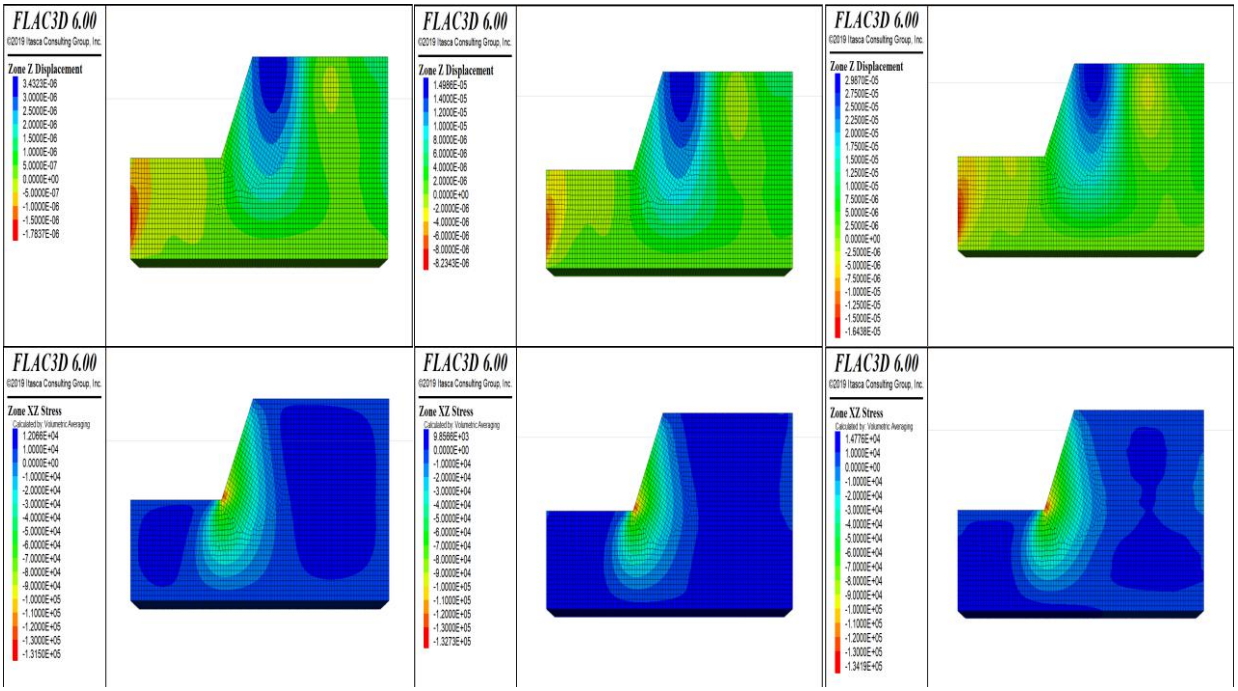

Figure 12. Analysis of overall displacement and acceleration of the model under the influence of LD seismic waves

Subsequent application of the aforementioned process to the Lushan seismic wave results in the generation of the relevant cloud diagrams. The relevant information is illustrated in Figure 13. As the input acceleration value increases, the maximum displacement value concomitantly rises. In this particular data set, the maximum displacement value is approximately 10 times the minimum displacement value. A simultaneous observation of the cloud diagram reveals that the maximum displacement value is distributed extensively throughout the primary structure of the model, indicating a high probability of substantial damage to the entire model. In real-world engineering operations, such seismic waves pose significant safety hazards, necessitating comprehensive protection measures for the associated slope construction areas.

It is imperative to observe the stress cloud of the slope model. The relevant information is shown in Figure 13. The model in the input acceleration 0.1g, 0.5g, 1.0g, the maximum stress value is $1.31*10^5$Pa, $1.31*10^5$Pa, $2.21*10^5$Pa. the model is subjected to the stress are in a similar interval, and the other seismic waves on the model, similar to the model, the model at the bottom of the slope also carries the model of the maximum stress. Therefore, it is necessary to pay attention to the stress at the bottom of the slopes in practical engineering.

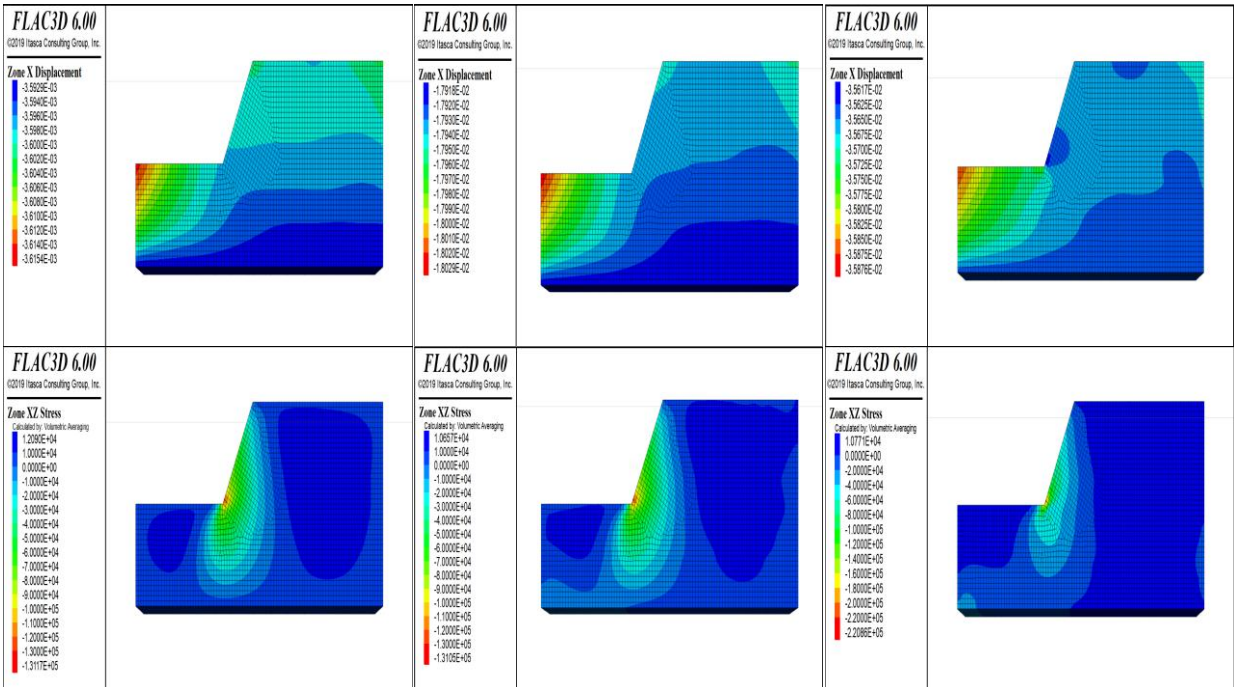

Figure 13. Comparison of slope shoulder and base acceleration under the influence of LS seismic waves

The experimental model of the Wolong seismic wave is then subjected to processing, employing the same methodology as outlined above. The relevant information is shown in Figure 14. As the input acceleration increases, the maximum displacement of the model also increases, following a consistent pattern. This set of data reveals a substantial numerical rise, with the final maximum displacement value being approximately 11 times the minimum displacement value. Upon observation of the presented cloud diagram, it is evident that the upper segment of the slope is susceptible to damage when subjected to the impact of seismic waves. Consequently, in the course of the engineering endeavours, reinforcement measures are implemented in the designated high-risk areas of the slope in order to mitigate damage incurred due to seismic waves.

In the following step of the research, the stress maps of the model are analysed. The relevant information is shown in Figure 14. the model is subjected to the maximum stress values of $1.31*10^5$Pa, $1.31*10^5$Pa, $1.30*10^5$Pa. respectively, when the input acceleration is 0.1g, 0.5g, 1.0g, and the slope has the same tendency of sliding downwards and collapsing, and the bottom of the model slope carries the maximum stresses of the model. Therefore, in the earthquake-prone phase, the detection and reinforcement of the stress condition at the bottom of the slope is indispensable for the stability of the whole slope.

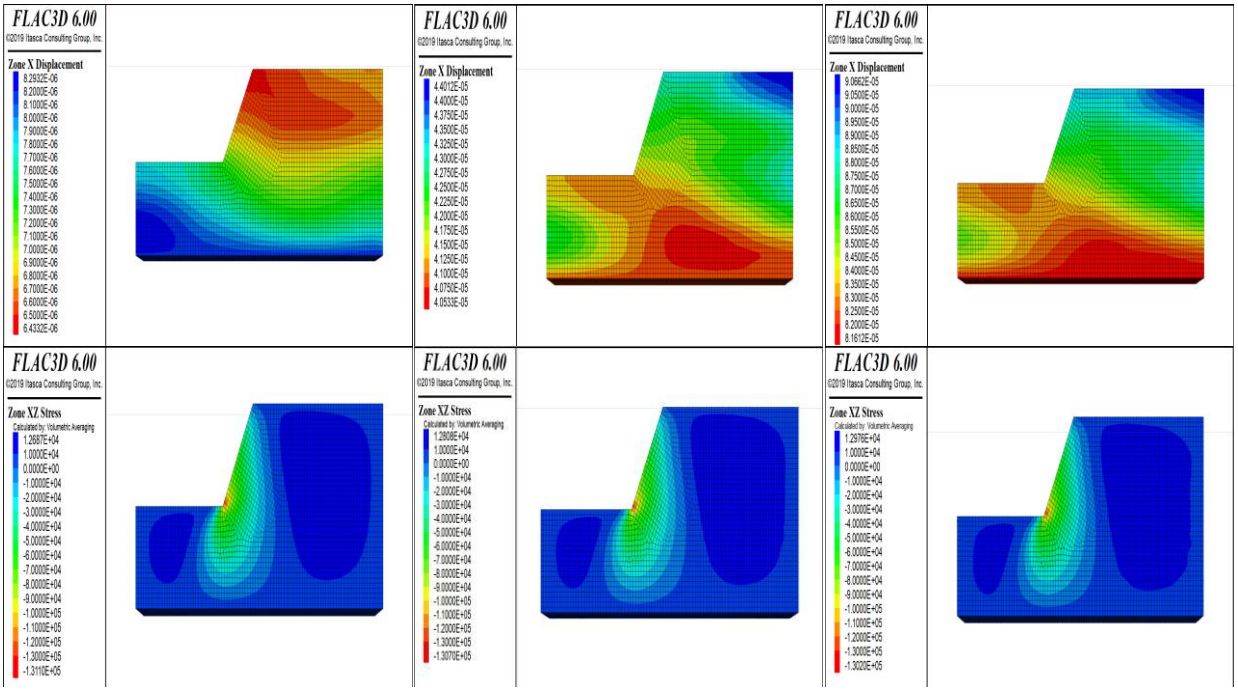

Figure 14. Comparison of acceleration at the shoulder and bottom of a slope under the influence of WL seismic waves

4.6. Comparison of stress changes at each detection point of the model under the influence of different seismic waves

The stress flow charts of slope shoulder. The relevant information is shown in Figure 15 (from left to right are Luding, Lushan, and Wolong, respectively), and the stress changes of the three kinds of seismic waves are investigated. Despite the distinct stress change characteristics exhibited by the three types of seismic waves, a unifying influence on the generalized slope model is observed. The analysis reveals that the slope's base receives the maximum stress value within the model, exhibiting a higher intensity of dynamic response compared to the other two monitoring points. The stress value at the middle of the slope is considerably smaller than that at the bottom of the slope with regard to both peak and average, and the stress value at the top of the slope changes very little and is subject to the least influence from the seismic wave. It can thus be seen that the influence of seismic waves on the slope model decreases slowly from near to far. Given these findings, it is imperative to emphasise the soil characteristics at the base of the slope, which is the most affected by seismic waves, in order to address the specific challenges posed by the soil in the given context.

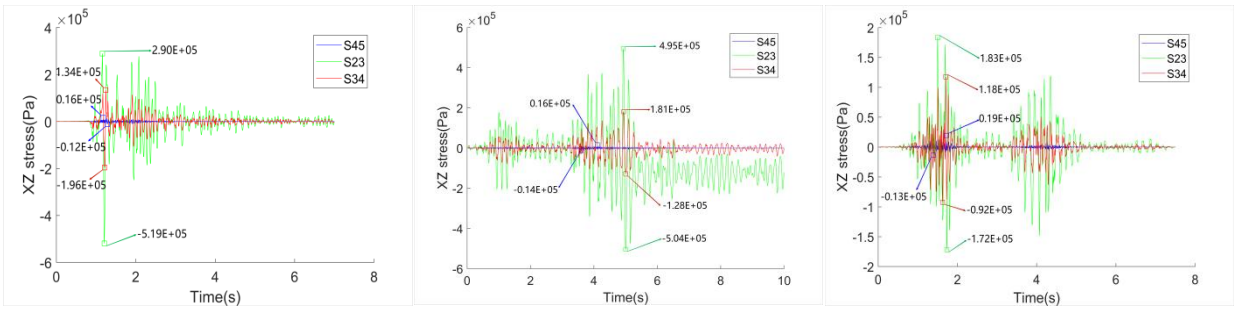

Figure 15. Stress changes at modeled monitoring sites under the influence of three types of seismic waves

5. Conclusions

In this experiment, through the model, using FLAC3D software, we studied the analysis of the dynamic response law of the slope under the action of multi-phase earthquakes, which lays the foundation for the study of slope stability and the subsequent seismic reinforcement measures.

1) The stress distribution, acceleration values and displacement response to the slope model are significantly different for different seismic waves, so the damage caused to the slope is different.

2) In the slope model, the displacement at the shoulder of the slope changes drastically under seismic action, and it is necessary to focus on the seismic reinforcement at the shoulder of the slope. The stress concentration at the bottom of the slope, the stability directly affects the overall slope safety, and needs to be synchronized to strengthen the protection. In the actual process, we should focus on reinforcing the corresponding area to avoid causing production accidents.

3) The actual engineering needs to comprehensively consider the geological conditions, hydrological environment and ground vibration parameters and other environmental complex factors. In the future experiments, we can combine the regional geological data with typical engineering cases to further study the actual situation and derive the corresponding research rules, so as to provide more accurate theoretical support for seismic design.

References

[1] Yang Jian, Zhang Hao, Shen Baocun, et al.Stability analysis and management of high and steep slopes in open pit mine discharge field based on finite element method——Take the example of the Shikobutai iron ore mine[J/OL].mineral exploration, 1-11[2025-01-13].

[2] Kong Bufan, Wan Huaining. Analysis of discrete element strength reduction method for slope stabilization[C]//Chinese Society of Rock Mechanics and Engineering.Abstracts of the 12th National Academic Conference on Rock Mechanics and Engineering.College of Civil Engineering and Transportation, Hohai University, 2012:1.

[3] Xu Jin, Zheng Shuying.Boundary element method for analyzing dynamic stability of slopes[J]. Journal of Northwest College of Architecture and Engineering (Natural Science Edition), 2000, (04): 72-75.

[4] Lu Shengliang. Numerical simulation analysis of the stability of surrounding rock in high extraction tunnel based on FLAC3D[J]. modernization of coal mining, 2025, 34(01): 52-57+65.

[5] Zhang Ning, Li Yulei, Li Zhehui, et al. Stability and reliability analysis of tailing pond dam slopes based on Monte-Carlo method[J]. uranium metallurgy, 2022, 41(03): 278-282.

[6] Du Xinguo. Evaluation method of rocky slope stability based on DDA[J]. Technology and Industry, 2023, 23(07): 177-182.

[7] Gen Yajie, Li Jiahen, Meng Xianjin, et al. Research on GRA-TOPSIS evaluation model of open pit mine slope stability based on variable weight theory[J]. Non-ferrous metal science and engineering, 24, 15(04): 553-560+569.

[8] Yuan Yin, Li Jiayu. Cusp mutation theory model for stability evaluation of rocky slopes[J]. Geology and exploration, 2021, 57(01): 183-189.

[9] Zhao Yibin, Zhang Yanfang, Jin Zhitong, et al. Characterization of the anomalous response of strain time series to earthquakes[J/OL]. Geodesy and geodynamics, 1-10[2025-01-16].

[10] Xie Chengyu, Liu Chengbo,Zhu Jiani, et al. Numerical simulation study on the safety of natural soil slope under multi-field coupling effect[J]. Journal of Xiangtan University (Natural Science Edition), 2021, 43(03): 94-105.